Numerical Heat Transfer, Part A, 57: 315–330, 2010

ISSN: 1040-7782 print/1521-0634 online
DOI: 10.1080/10407781003613323

INVERSE NATURAL CONVECTION PROBLEM WITH RADIATION IN RECTANGULAR ENCLOSURE

Yun Ky Hong[1], Seung Wook Baek[1], and Man Young Kim[2]
[1]*Department of Aerospace Engineering, School of Mechanical, Aerospace and Systems Engineering, Korea Advanced Institute of Science and Technology, Taejon, Korea*
[2]*Department of Aerospace Engineering, Chonbuk National University, Chonbuk, Korea*

Inverse thermal problem is applied to natural convective flow with radiative heat transfer. The bottom wall temperature in the 2-D cavity domain is estimated by using gas temperature measurements in the flow field. The inverse problem is solved through a minimization of an objective function using the conjugate gradient method with adjoint problem. The effects of functional form of bottom wall temperature profile, the number and the position of measurement points, and the measurement errors are investigated and discussed. The conjugate gradient method is found to work well in estimating the bottom wall temperature, even when natural convection with radiation phenomena is involved.

1. INTRODUCTION

The inverse problem has various application possibilities in the science and engineering fields, but the inverse problem may not always be solved due to its intrinsic ill-posed nature. Its ill-posed nature makes many algorithms used for direct problems inapplicable to inverse problems, so that peculiar numerical schemes must be applied to stabilize the solution.

Among others, there is literature that considers the inverse convection problem. The most commonly solved problem is duct flow. In these problems, the temperature or heat flux information is used to estimate the wall or inlet conditions. Huang and Özisik [1] estimated the wall heat flux in forced convection. Li and Yan determined the wall heat flux for laminar flow in an annular duct [2], and for the turbulent flow in a parallel plate duct [3]. For a similar condition, Liu and Özisik [4] estimated the spatially varying inlet temperature profile, while Bokar and Özisik [5] estimated the temporally varying inlet temperature profile. Recently, Park and

Received 30 June 2009; accepted 20 December 2009.
This work was supported by the Korean Science and Engineering Foundation (KOSEF) grant funded by the Korean Government (MEST) (No. 2009-0079086).
Address correspondence to Seung Wook Baek, Department of Aerospace Engineering, School of Mechanical, Aerospace and Systems Engineering, Korea Advanced Institute of Science and Technology, 373-1 Guseong-dong, Yuseong-gu, Daejeon 305-701, Republic of Korea. E-mail: swbaek@kaist.ac.kr

NOMENCLATURE

c	specific heat, $J/(kg \cdot K)$	β	extinction coefficient, i.e., sum of absorption and scattering coefficient, m^{-1}
d^k	direction of descent at kth iteration	β^k	search step size at kth iteration
F	bottom wall temperature distribution	δ	Dirac delta function
H, L	height and length of domain	ε	convergence criterion
I	radiative intensity	ε_ω	wall emissivity
k	conductivity, $W(m \cdot K)$	γ^k	conjugation coefficient at kth iteration
M	the number of sensors	κ	absorption coefficient, m^{-1}
g	acceleration of gravity	ρ	density, kg/m^3
G	nondimensional radiative intensity	ρ_w	wall reflectivity
N	conduction to radiation parameter	μ	viscosity
Pe, Ra, Re	nondimensional variable	σ	standard deviation
O, Q, R, U, V	Lagrange multiplier	σ_{SB}	Stefan-Boltzmann constant
S	objective function	τ	optical thickness
T	nondimensional temperature	ω	random number
$T^*_{\text{ref.}}$	reference temperature, T_w	Ω	solid angle
ΔT	sensitivity function	**Superscript**	
u, v	nondimensional velocity	k	number of iteration
u^*_{mean}	representative velocity, $\mu/(\rho \cdot L)$	*	dimensional variable
x, y	nondimensional length variable	**Subscript**	
Y	measured temperature	b	black body
α	thermal expansion coefficient, K^{-1}	m	mth measurement point
		mean	average value
		R	radiation
		w	wall

Chung [6] solved the natural convection problem. They found the heat source at the given point by using temperature information.

On the other hand, there is limited literature relating to the inverse radiation problem. Li [7] estimated thermal properties by considering conduction and radiation, whereas Park and Yoon [8] and Park and Yoo [9] found the radiative properties and the temporally varying heat source in a three-dimensional domain, respectively. There were also inverse radiation problems which were studied by Kim and Baek [10], Li [11], and Hong and Baek [12, 13].

Based on these previous works, a more complicated inverse problem is considered. The natural convection problem has many engineering applications. So, in this study, the inverse natural convection and radiation problem is considered. Initially, there is stationary flow in the cavity domain. When only a part of the bottom wall is heated up, a natural convective flow is induced because of the buoyancy. Consequently, the fluid flow rotates in the cavity as heat is continuously transferred from the bottom wall to fluid. Given gas temperature measurements in the flow regime, the bottom wall temperature can be determined.

There are many methods applicable to solve the inverse problem, but the most commonly used method is the conjugate gradient method [14]. Especially,

the conjugate gradient method with adjoint problem is strongly recommended because it doesn't require time-consuming sensitivity coefficient calculations. So, the conjugate gradient method with adjoint problem is employed in this study.

2. FORMULATION

2.1. Direct Problem

A steady natural convection and radiation flow is considered, as shown in Figure 1. When the bottom wall is partially heated up, the hot flow will rise due to the buoyancy and be cooled by the cold wall. In this study, thermofluid dynamic properties of fluid are assumed to be temperature independent, while the radiative heat transfer is taken into account.

We define the following nondimensional variables.

$$x = \beta x^*, \quad y = \beta y^*, \quad T = \frac{T^*}{T^*_{\text{ref}}}, \quad u = \frac{u^*}{u^*_{\text{mean}}}, \quad v = \frac{v^*}{u^*_{\text{mean}}}, \quad p = \frac{p^*}{\rho u^{*2}_{\text{mean}}}$$

$$\text{Ra} = \frac{g\alpha T^*_{\text{ref}}}{\beta u^{*2}_{\text{mean}}}, \quad \text{Re} = \frac{\rho u^*_{\text{mean}}}{\mu\beta}, \quad \text{Pe} = \frac{\rho c u^*_{\text{mean}}}{k_g\beta}, \quad G = \frac{I^*}{\sigma_{SB} T^{*4}_{\text{ref}}}, \quad N = \frac{k_g\beta}{4\sigma_{SB} T^{*3}_{\text{ref}}} \tag{1}$$

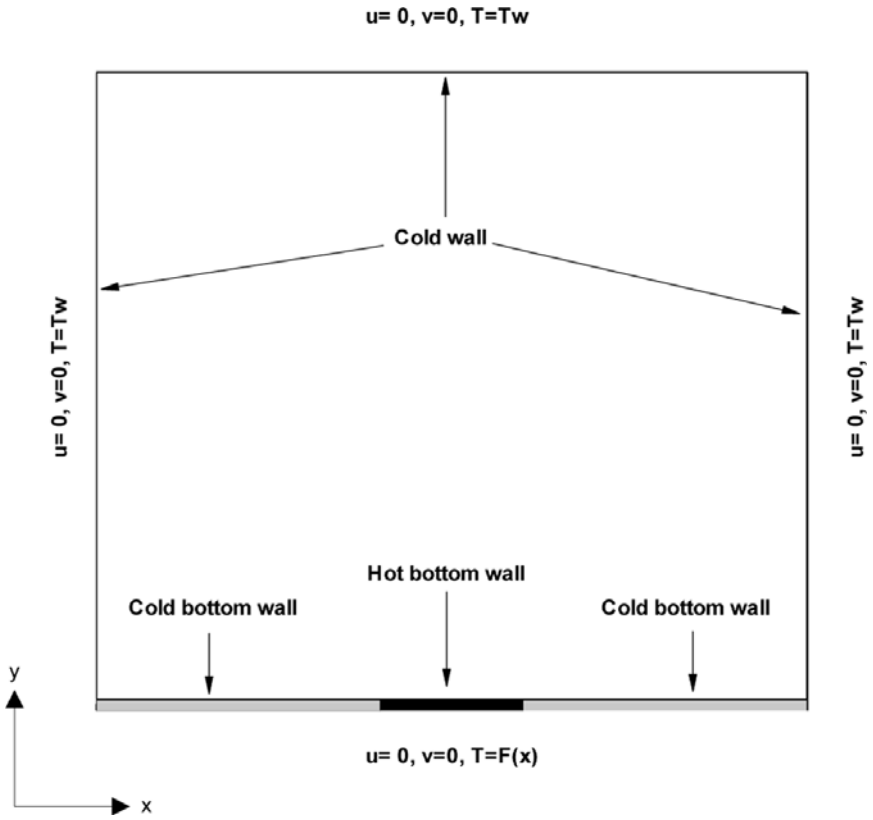

Figure 1. Problem geometry and boundary conditions.

where the superscript asterisk means the dimensional variables. The governing equations can be represented by [15]

$$\frac{\partial u}{\partial x}+\frac{\partial v}{\partial y}=0 \tag{2a}$$

$$u\frac{\partial u}{\partial x}+v\frac{\partial u}{\partial y}=-\frac{\partial p}{\partial x}+\frac{1}{\mathrm{Re}}\left(\frac{\partial^2 u}{\partial x^2}+\frac{\partial^2 u}{\partial y^2}\right) \tag{2b}$$

$$u\frac{\partial v}{\partial x}+v\frac{\partial v}{\partial y}=-\frac{\partial p}{\partial y}+\frac{1}{\mathrm{Re}}\left(\frac{\partial^2 v}{\partial x^2}+\frac{\partial^2 v}{\partial y^2}\right)+\mathrm{Ra}(T-T_{\mathrm{sys}}) \tag{2c}$$

$$\mathrm{Pe}\left(u\frac{\partial T}{\partial x}+v\frac{\partial T}{\partial y}\right)=\left(\frac{\partial^2 T}{\partial x^2}+\frac{\partial^2 T}{\partial y^2}\right)-\nabla\cdot\vec{q}_R \tag{2d}$$

$$\frac{dG(\vec{\tau})}{d\tau}=G_b-G(\vec{\tau}) \tag{2e}$$

Here, the system temperature, the divergence of radiative heat flux, and black body intensity are, respectively, given by

$$T_{\mathrm{sys}}=\frac{1}{2}(T_{\mathrm{hot}}+T_{\mathrm{cold}}) \tag{3a}$$

$$\nabla\cdot\vec{q}_R=\frac{\kappa}{N\beta}\left(T^4-\frac{1}{4}\int G(\vec{s})d\Omega\right) \tag{3b}$$

$$G_b=\frac{T^4}{\pi} \tag{3c}$$

In order to close the current problem by using the equation set above, the following boundary conditions are needed.

$$x=x_0,\ x_f,\quad u=v=0,\quad T=T_w=300\,\mathrm{K},$$

$$y=y_f,\quad u=v=0,\quad T=T_w=300\,\mathrm{K}$$

$$y=y_0,\quad u=v=0,\quad T=F(x)$$

$$G(\vec{\tau})=\frac{\varepsilon_w}{\pi}T^4_{\mathrm{boundary}}+\frac{\rho_w}{\pi}\int_{\vec{n}\cdot\vec{\tau}'<0}\left|\vec{n}\cdot\vec{\tau}'\right|G(\vec{\tau}')d\Omega',\quad(\vec{n}\cdot\vec{\tau}'>0) \tag{4}$$

The radiative transfer equation mentioned above is solved using the discrete ordinates method (S_4 approximation) [15].

2.2. Inverse Problem

For the inverse problem, the bottom temperature profile $F(x)$ is regarded as unknown. It is to be determined by using the temperature measurements using M sensors located at appropriate locations (x_m, y_m), $m = 1, \ldots, M$ in the cavity. The conjugate gradient method (CGM) is applied to minimize the following functional.

$$S(F(x)) = \sum_{m=1}^{M} [Y_m(x, y) - T(x_m, y_m; F(x))]^2 \tag{5}$$

where Y_m and T are measured and estimated nondimensional fluid temperature at the measurement locations. The estimated temperature T is the solution of the direct problem by assuming the bottom wall temperature profile $F(x)$. Two auxiliary problems are required for the successful implementation of the CGM: the sensitivity problem and the adjoint problem.

Sensitivity problem. To obtain the sensitivity problem, it is assumed in the direct problem that when $F(x)$ undergoes a small increment $\Delta F(x)$, the velocity u and v, the pressure p, the temperature T, and the intensity G change by Δu, Δv, Δp, ΔT, and ΔG, respectively. From this assumption, the following sensitivity problem is obtained.

$$\frac{\partial \Delta u}{\partial x} + \frac{\partial \Delta v}{\partial y} = 0 \tag{6a}$$

$$\Delta u \frac{\partial u}{\partial x} + u \frac{\partial \Delta u}{\partial x} + \Delta v \frac{\partial u}{\partial y} + v \frac{\partial \Delta u}{\partial y} = -\frac{\partial \Delta p}{\partial x} + \frac{1}{\mathrm{Re}} \left(\frac{\partial^2 \Delta u}{\partial x^2} + \frac{\partial^2 \Delta u}{\partial y^2} \right) \tag{6b}$$

$$\Delta u \frac{\partial v}{\partial x} + u \frac{\partial \Delta v}{\partial x} + \Delta v \frac{\partial v}{\partial y} + v \frac{\partial \Delta v}{\partial y} = -\frac{\partial \Delta p}{\partial y} + \frac{1}{\mathrm{Re}} \left(\frac{\partial^2 \Delta v}{\partial x^2} + \frac{\partial^2 \Delta v}{\partial y^2} \right) + \mathrm{Ra} \Delta T \tag{6c}$$

$$\mathrm{Pe}\left(\Delta u \frac{\partial T}{\partial x} + \Delta v \frac{\partial T}{\partial y} \right) + \mathrm{Pe}\left(u \frac{\partial \Delta T}{\partial x} + v \frac{\partial \Delta T}{\partial y} \right) = \left(\frac{\partial^2 \Delta T}{\partial x^2} + \frac{\partial^2 \Delta T}{\partial y^2} \right) - \frac{\kappa}{N\beta} \left(4T^3 \Delta T - \frac{1}{4} \int \Delta G(\vec{s}) d\Omega \right) \tag{6d}$$

$$\frac{d\Delta G(\vec{\tau})}{d\tau} = \frac{4}{\pi} T^3 \Delta T - \Delta G(\vec{\tau}) \tag{6e}$$

And the boundary conditions are given by following equations.

$$\begin{aligned} &x = x_0,\ x_f \quad \Delta u = \Delta v = 0 \quad \Delta T = 0 \\ &y = y_f \quad \Delta u = \Delta v = 0 \quad \Delta T = 0 \\ &y = y_0 \quad \Delta u = \Delta v = 0 \quad \Delta T(x, y_0) = \Delta F \end{aligned}$$

$$\Delta G(\vec{\tau}) = \frac{4\varepsilon_w}{\pi} T^3 \Delta T + \frac{\rho_w}{\pi} \int_{\vec{n} \cdot \vec{\tau}' < 0} |\vec{n} \cdot \vec{\tau}'| \Delta G(\vec{\tau}') d\Omega', \quad (\vec{n} \cdot \vec{\tau}' > 0) \tag{7}$$

Adjoint problem and gradient equation. To derive the adjoint problem, Eqs. (2*a*)–(2*e*) are multiplied by the Lagrange multipliers $O(x, v)$, $Q(x, y)$, $R(x, y)$, $U(x, y)$, and $V(x, y, \Omega)$. Each resulting expression is integrated over the space domain, and then added to the right-hand side of objective function to yield the following.

$$
\begin{aligned}
S(F(x)) = \sum_{m=1}^{M} [Y_m(x,y) - T(x_m, y_m; F(x))]^2 &- \int_x \int_y O(x,y)\left[\frac{\partial u}{\partial x} + \frac{\partial v}{\partial y}\right] dxdy \\
&- \int_x \int_y Q(x,y)\left[u\frac{\partial u}{\partial x} + v\frac{\partial u}{\partial y} + \frac{\partial p}{\partial x} - \frac{1}{\mathrm{Re}}\left(\frac{\partial^2 u}{\partial x^2} + \frac{\partial^2 u}{\partial y^2}\right)\right] dxdy \\
&- \int_x \int_y R(x,y)\left[u\frac{\partial v}{\partial x} + v\frac{\partial v}{\partial y} + \frac{\partial p}{\partial y} - \frac{1}{\mathrm{Re}}\left(\frac{\partial^2 v}{\partial x^2} + \frac{\partial^2 v}{\partial y^2}\right) - \mathrm{Ra}(T - T_{\mathrm{sys}})\right] dxdy \\
&- \int_x \int_y U(x,y)\left[\mathrm{Pe}\left(u\frac{\partial T}{\partial x} + v\frac{\partial T}{\partial y}\right) - \left(\frac{\partial^2 T}{\partial x^2} + \frac{\partial^2 T}{\partial y^2}\right) + \nabla \cdot \vec{q}_R\right] dxdy \\
&- \int_x \int_y \int_\Omega V(x,y,\Omega)\left[\frac{dG(\tau)}{d\tau} - G_b + G(\tau)\right] d\Omega dxdy
\end{aligned} \tag{8}
$$

Next, the variation $\Delta S(F(x))$ is obtained. After some algebraic manipulations, the resulting expressions are allowed to go to zero. Thereby, the following adjoint problem is obtained to determine the Lagrange multiplier $O(x, v)$, $Q(x, y)$, $R(x, y)$, $U(x, y)$, and $V(x, y, \Omega)$ such that

$$
\frac{\partial Q}{\partial x} + \frac{\partial R}{\partial y} = 0 \tag{9a}
$$

$$
u\frac{\partial Q}{\partial x} + v\frac{\partial Q}{\partial y} = -\frac{\partial O}{\partial x} - \frac{1}{\mathrm{Re}}\left(\frac{\partial^2 Q}{\partial x^2} + \frac{\partial^2 Q}{\partial y^2}\right) + Q\frac{\partial u}{\partial x} + R\frac{\partial v}{\partial x} + \mathrm{Pe}\,U\frac{\partial T}{\partial x} \tag{9b}
$$

$$
u\frac{\partial R}{\partial x} + v\frac{\partial R}{\partial y} = -\frac{\partial O}{\partial y} - \frac{1}{\mathrm{Re}}\left(\frac{\partial^2 R}{\partial x^2} + \frac{\partial^2 R}{\partial y^2}\right) + Q\frac{\partial u}{\partial y} + R\frac{\partial v}{\partial y} + \mathrm{Pe}\,U\frac{\partial T}{\partial y} \tag{9c}
$$

$$
\begin{aligned}
\mathrm{Pe}\left(u\frac{\partial U}{\partial x} + v\frac{\partial U}{\partial y}\right) = &-\left(\frac{\partial^2 U}{\partial x^2} + \frac{\partial^2 U}{\partial y^2}\right) - R\mathrm{Ra} + \frac{4\kappa}{N\beta}T^3 U - \frac{4}{\pi}T^3 \int_\Omega V d\Omega \\
&+ \sum_{m=1}^{M} 2[Y_m - T_g]\delta(x - x_m)\delta(y - y_m)
\end{aligned} \tag{9d}
$$

$$
\frac{dV(\vec{\tau})}{d\tau} = -\frac{\kappa_g}{4N\beta}U + V(\vec{\tau}) \tag{9e}
$$

where $\delta(\ )$ is the Dirac delta function, and the boundary conditions for the above equations are

$$\begin{aligned} x = x_0, x_f \quad Q = R = 0 \quad U = 0 \quad V = 0 \\ y = y_0, y_f \quad Q = R = 0 \quad U = 0 \quad V = 0 \end{aligned} \tag{10}$$

The gradient direction of the objective function is determined by

$$\nabla S[F(x)] = \left.\frac{\partial U}{\partial y}\right|_{x,y_0} \tag{11}$$

This is the gradient equation that relates the gradient of the functional $S[F(x)]$ to the Lagrange multipliers.

Iterative procedure. Assuming that all dependent variables and $\nabla S[F(x)]$ are available at the kth iteration, the iterative procedure is performed as follows. The boundary temperature at step $k+1$ is computed from

$$F^{k+1}(x) = F^k(x) - \beta^k \mathbf{d}^k(x) \tag{12}$$

where $\mathbf{d}^k$ is the direction of descent which is determined from

$$\mathbf{d}^k = \nabla S[F^k(x)] + \gamma^k \mathbf{d}^{k-1} \tag{13}$$

and the conjugation coefficient γ^k is obtained from the Fletcher-Reeves expression [14] such that

$$\gamma^k = \frac{\int_x \{\nabla S[F^k(x)]\}^2 dx}{\int_x \{\nabla S[F^{k-1}(x)]\}^2 dx} \quad \text{with } \gamma^0 = 0 \tag{14}$$

The search step size β^k is obtained by minimizing the functional given by Eq. (5) with respect to β^k such that

$$\beta^k = \frac{\sum_{m=1}^{M} [T(x_m, y_m; F^k(x)) - Y_m] \Delta T(x_m, y_m; \mathbf{d}^k)}{\sum_{m=1}^{M} [\Delta T(x_m, y_m; \mathbf{d}^k)]^2} \tag{15}$$

where $T(x_m, y_m; \mathbf{d}^k)$ is the solution of the sensitivity problem which is obtained by setting $\Delta F(y) = \mathbf{d}^k$

Discrepancy principle for stopping criterion. If the problem contains no measurement error, the traditional check condition is specified by

$$S(F^{k+1}(x)) < \varepsilon \tag{16}$$

where the value of the tolerance ε is chosen such that sufficiently stable solutions are obtained. However, the observed temperature data contains some measurement

errors. As the estimated temperatures approach the measured temperatures that contain some errors, a large oscillation may appear during the minimization of the function (Eq. (5)) in the inverse solution, thereby resulting in an ill-posed nature for the inverse problem. However, the CGM may become well-posed if the discrepancy principle is used to stop the iterative procedure. When the residuals between measured and estimated temperatures are of the same order of magnitude of ε such that

$$|Y(x_{\text{measured}}, y_{\text{measured}}) - T(x_{\text{measured}}, y_{\text{measured}})| \approx \sigma \tag{17}$$

where σ is the standard deviation of the measurements which is assumed to be a constant. The following expression is obtained for stopping criteria ε by substituting Eq. (17) into Eq. (5).

$$\varepsilon = \sum_{m=1}^{M} \sigma^2 = M\sigma^2 \tag{18}$$

Then, the stopping criterion is given by Eq. (16) with ε determined from Eq. (18).

3. RESULTS AND DISCUSSION

Now, the bottom wall temperature condition is to be predicted when measurements for gas temperature are available in the flow regime in the presence of convection and radiation. The computational accuracy of the present inverse analysis is examined. A test function is considered with simulated measurements Y_{measured}. The estimated bottom wall temperature is then compared with the exact one. The length of domain, L, is 0.1 m and height, H, is 0.1 m. The grid system is 241×241. The gas properties are $\rho_g = 0.4975\,\text{kg/m}^3$, $c_g = 1075\,\text{J/kg}\cdot\text{K}$, $k_g = 0.0524\,\text{W/m}\cdot\text{K}$, and $\kappa = 0.1\,\text{m}^{-1}$. The corresponding Reynolds number, Rayleigh number, and Pelect number are about 13,000, 5,000, and 9,000, respectively.

The simulated measured gas temperature data, Y_{measured}, are generated by adding some random errors to the computed exact temperatures as follows.

$$Y_{\text{measured}} = T_{\text{exact}} + \omega\sigma \tag{19}$$

where σ is the selected standard deviation which takes values of 4.0 K and 8.0 K, while ω is a random number between $-2.576 \le \omega \le 2.576$, which represents 99% confidence bound for the measured temperature.

Two types of functional form for $F(x)$ are selected as follows:

(1)
$$F(x) = 600 \sin\left(\frac{x - 0.045}{0.01}\pi\right) + 300 \quad (0.045\,\text{m} < x < 0.055\,\text{m})$$
$$F(x) = 300 \quad (0.0\,\text{m} \le x < 0.045\,\text{m} \text{ and } 0.055\,\text{m} < x \le 0.1\,\text{m}) \tag{20a}$$

(2)
$$F(x) = 700 \quad (0.04\,\text{m} < x < 0.06\,\text{m})$$
$$F(x) = 300 \quad (0.0\,\text{m} \le x < 0.0475\,\text{m} \text{ and } 0.0525\,\text{m} < x \le 0.1\,\text{m}) \tag{20b}$$

where x and $F(x)$ are dimensional variables. These two test functions are shown in Figure 2.

The direct problem is validated by solving the natural convection problem as obtained by Poots [16]. The vertical wall of rectangular enclosure is heated, whereas the other walls are cooled. The heat flux is calculated for various Grashof numbers. A comparison of the results is shown in Figure 3. The present Nusselt number distribution is almost the same as that of Poots [16].

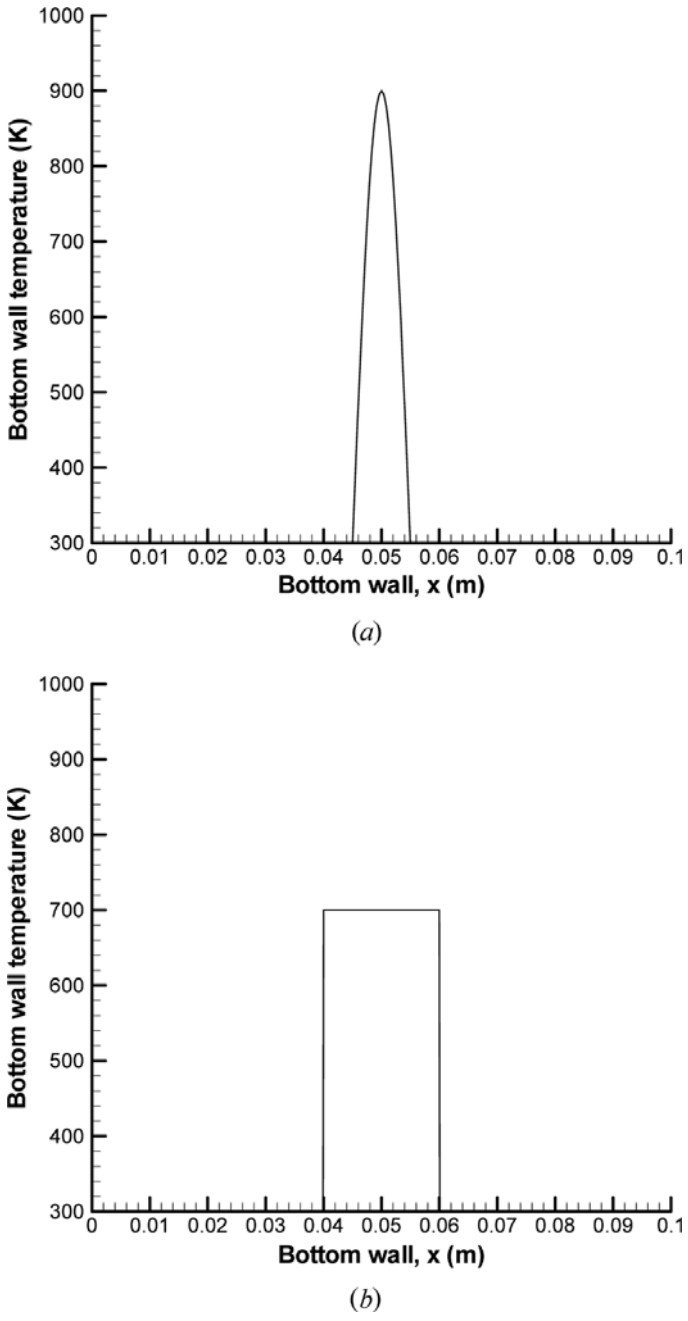

Figure 2. Two test cases for the bottom wall temperature distribution. (*a*) Test function (1)—sinusoidal variation of wall temperature and (*b*) test function (2)—stepwise variation of wall temperature.

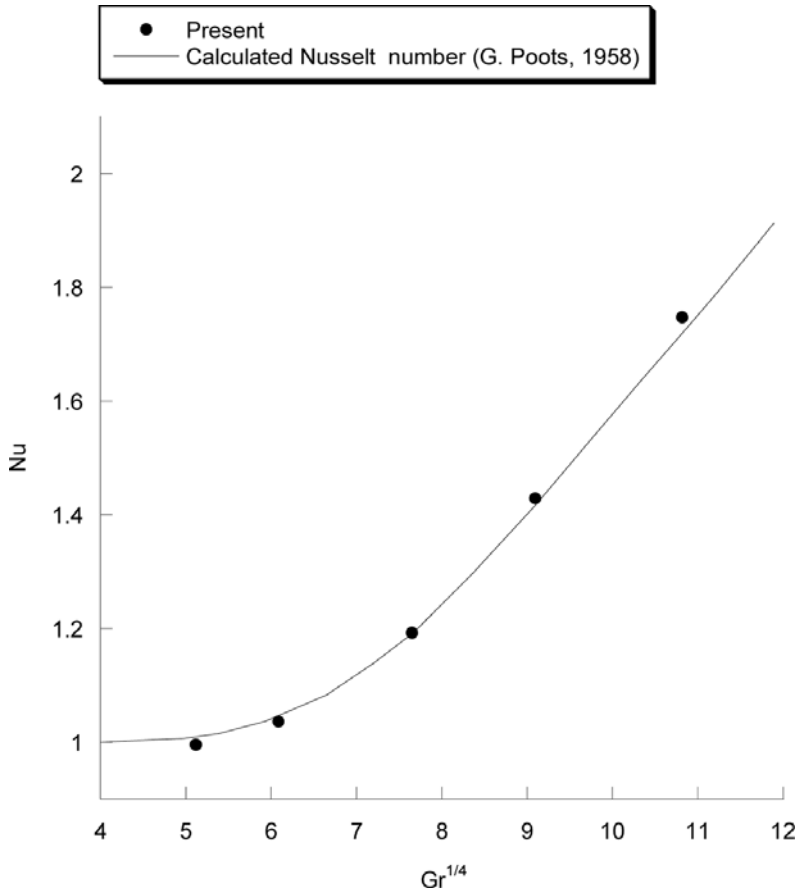

Figure 3. Variation of the Nusselt number with Grashof number.

Figure 4 shows the streamline when the center part of the bottom wall is heated up like test function (1). The hot region of the bottom wall is represented by the black region, while the cold region of the bottom wall is represented by the gray region. The heated gas of the center region goes up while the cooled gas near the side wall falls down. Almost similar flow motion is shown for the heated bottom wall of test function (2).

In order to estimate the effect of measurement error, the number of measurement points and measurement positions are fixed. The number of measurement points is 5, while the measurement positions are located at grid numbers of (111,15), (116,15), (121,15), (126,15), and (131,15). The simulated measurement values are listed in Table 1. These are uniformly distributed from the center position and located 2 mm above the bottom wall. Figure 5 illustrates the estimated bottom wall temperature for the test function (1). The solid line shows the exact solution, whereas the dotted and dash-dotted lines represent the results when the measurement error is 4.0 K and 12.0 K, respectively. Regardless of measurement error, the overall test function contour is found to be successfully estimated. Based on this fact, the CGM method is considered to be very useful for this radiative as well as convective flow inverse problem even with some measurement error. In this figure, the asymmetry is also observed since each local position is inversely calculated. Figure 6 shows the estimated heat flux for test case one. While the positive

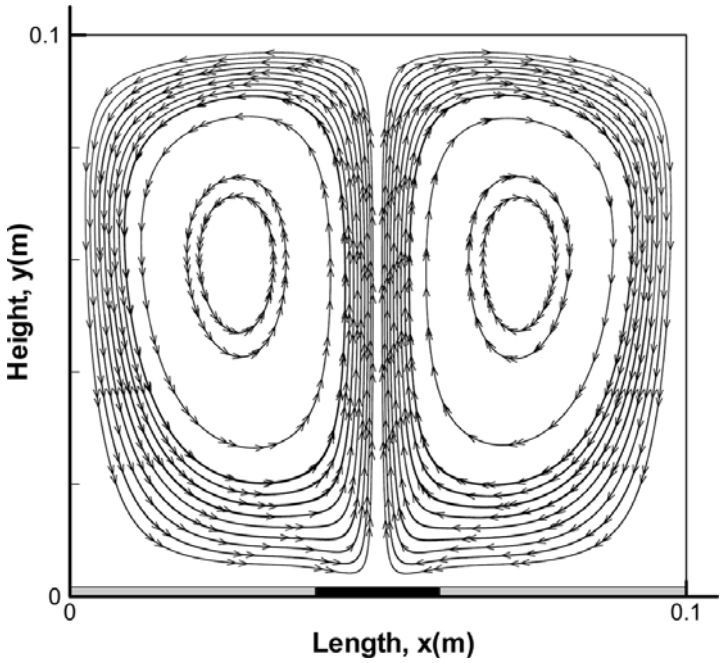

Figure 4. The streamline in the cavity domain for test case (1).

heat flux represents the heat flux from the gas, the negative one is the heat flux from the bottom wall.

The effect of measurement error is also investigated for the test function (2). Figure 7 shows the estimated bottom wall distribution. The number of sensors is 9 and the sensor locations are at grid numbers of (101,15), (106,15), (111,15), (116,15), (121,15), (126,15), (131,15), (136,15), and (141,15). Compared with test function (1), the results show a smaller difference when the measurement error is 4.0 K and 12.0 K; and, actually, the temperature distribution determined is more inaccurate compared with the exact solution than that in test function (1) since the temperature distribution is discontinuous.

From Figures 5 and 7, it can be found that the inverse estimation is inaccurate when the bottom wall temperature has a stepwise variation like in test function (2).

Table 1. Simulated measured values for test case (1)

Measurement error	Grid point number of sensor locations	Simulated measured values (K)
4	(111,15)	410.6
	(116,15)	555.6
	(121,15)	662.5
	(126,15)	556.8
	(131,15)	396.5
12	(111,15)	421.2
	(116,15)	543.8
	(121,15)	676.7
	(126,15)	547.0
	(131,15)	378.7

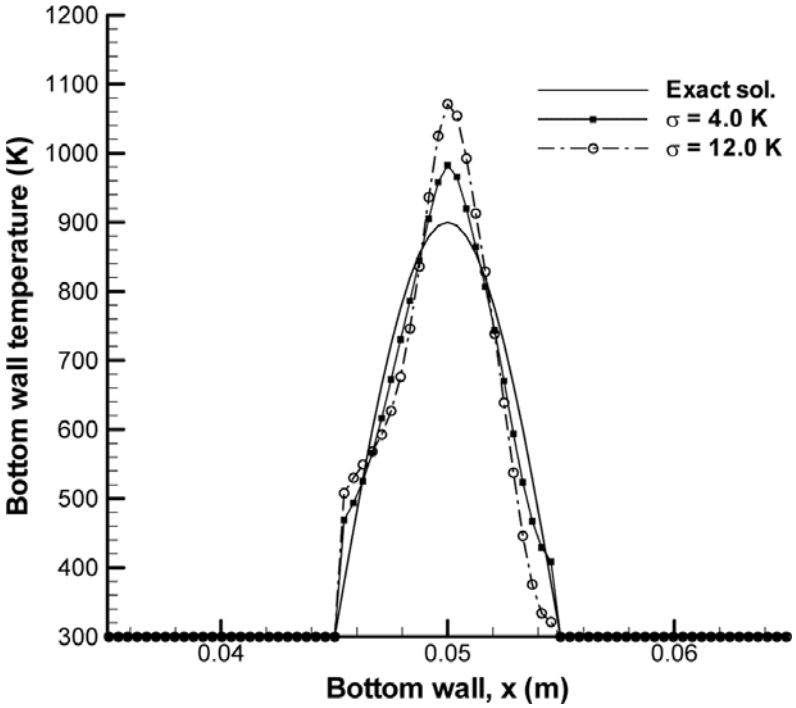

Figure 5. Effect of measurement error for test case (1): temperature estimation.

Consequently, in the following discussion, only the test function (1) is considered for further numerical experiments.

Figure 8 illustrates the estimated bottom wall temperature in which the number of measurement points is changed. In this case, the measurement error is fixed at

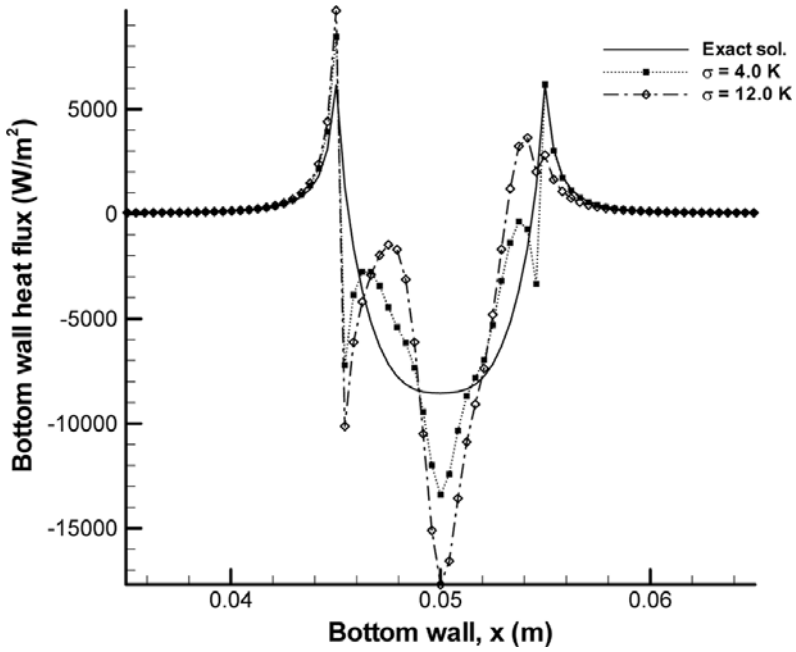

Figure 6. Effect of measurement error for test case (1): heat flux estimation.

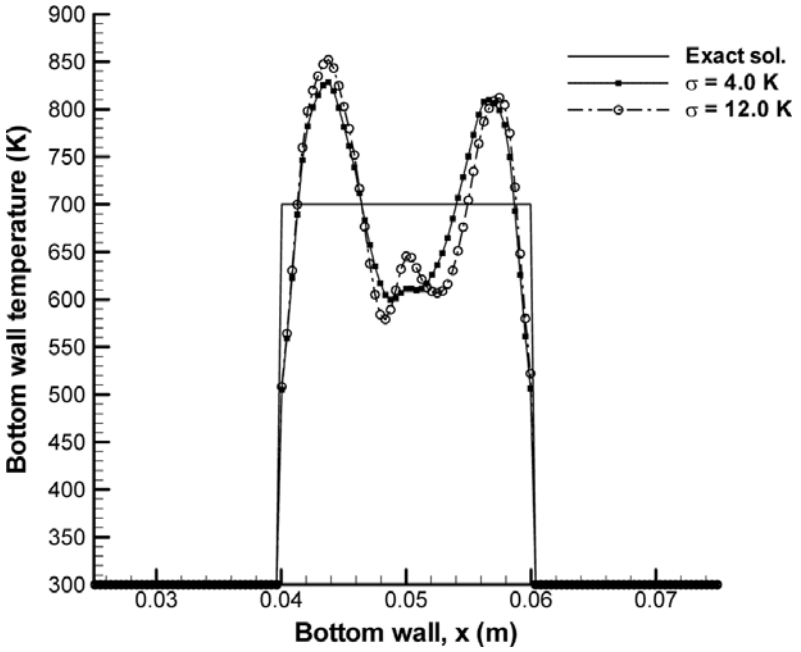

Figure 7. Effect of measurement error for test case (2).

4.0 K. This figure shows that nine measurement sensors yield the most accurate results. When the number of measurement sensor is only one, the results are most inaccurate because the measurement information is insufficient.

The measurement sensor locations are vertically changed in Figure 9. In this figure, the measurement error is fixed at 4.0 K and the x-directional measurement

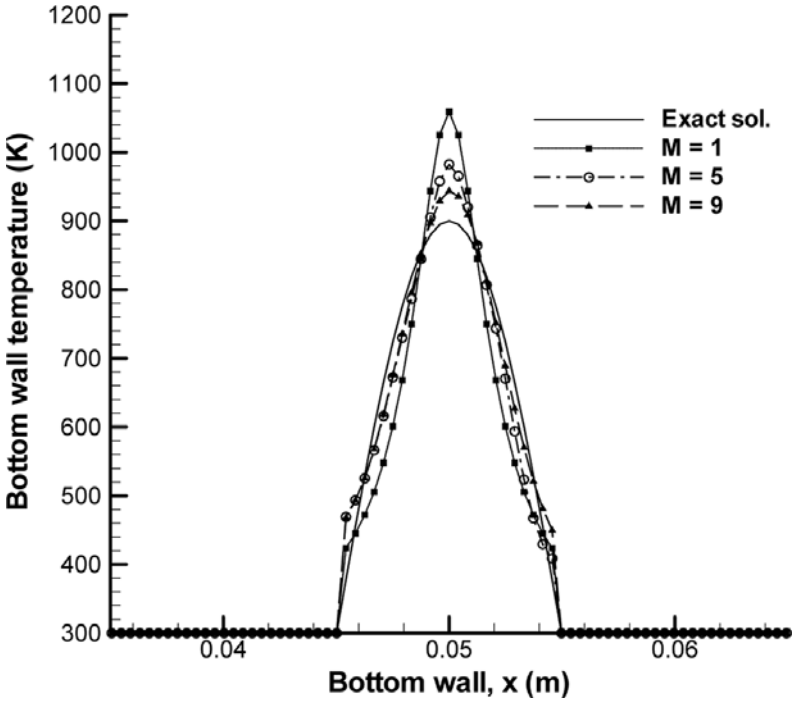

Figure 8. Effect of the number of measurement points for test case (1).

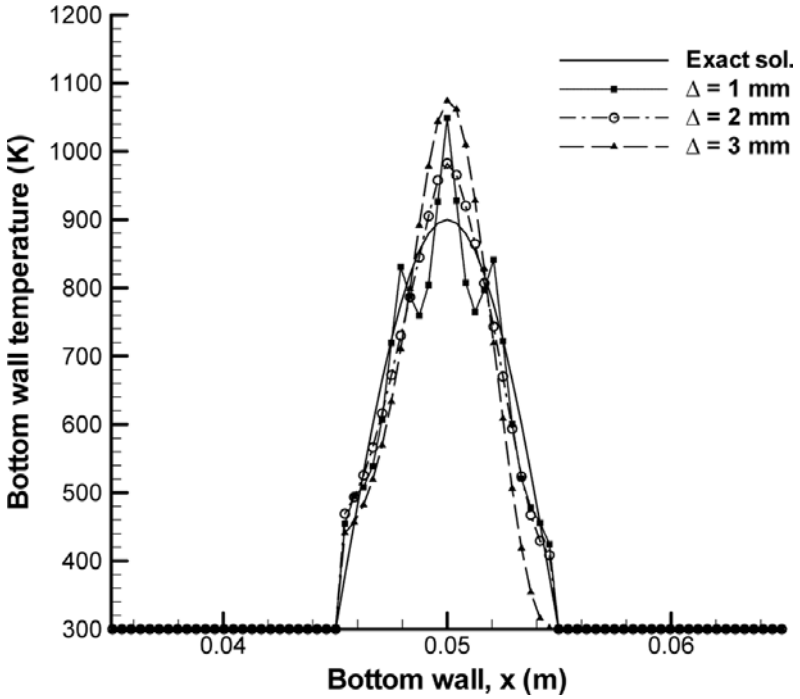

Figure 9. Effect of vertically different measurement positions for test case (1).

positions are also fixed at grids of 111, 116, 121, 126, and 131. The symbol, Δ, represents the distance from the bottom wall to the sensor locations. When the sensors are located 2 mm above the bottom wall, the inverse results are best. When the sensor location is 3 mm away from the bottom wall, the estimated temperature is mostly poor.

The horizontal position of measurement sensors is also changed. Table 2 shows the sensor locations, while Figure 10 shows the estimated results. In this figure, the measurement error is also fixed at 4.0 K. When the sensors are all located on the left-hand side of the center position as in cases (4) and (5), the inverse solutions are very poor. The sensor at the center position is observed to

Table 2. Sensor locations in x

Case number	Grid point number (distance from the center position (mm)), of sensor locations
Case 1	111, 116, 121, 126, 131 (−4.2, −2.1, 0, 2.1, 4.2)
Case 2	106, 111, 116, 121, 126 (−6.3,−4.2,−2.1, 0, 2.1)
Case 3	101, 106, 111, 116, 121 (−8.4,−6.3,−4.2, −2.1, 0)
Case 4	96, 101, 106, 111, 116 (−10.5,−8.4,−6.3,−4.2, −2.1)
Case 5	91, 96, 101, 106, 111 (−12.6,−10.5,−8.4,−6.3,−4.2)

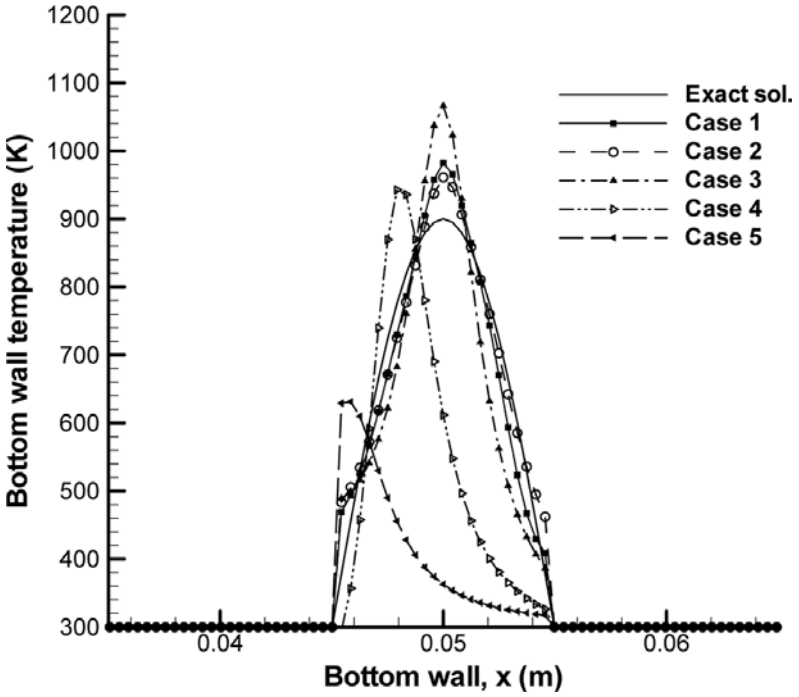

Figure 10. Effect of horizontally different measurement positions for test case (1).

play an important role in determining the temperature distribution at the bottom wall, as in cases (1)–(3).

4. CONCLUSION

In this study, an inverse natural convection problem with radiative phenomena was studied using the conjugate gradient method. The heated bottom wall temperature distribution was inversely estimated. In order to examine the effects of measurement error and locations on two functional forms of wall temperature distribution, various numerical experiments were done.

In conclusion, the conjugate gradient method with adjoint problem was found to be very successful in inversely predicting the bottom wall temperature profile even if the thermal radiation, which was of elliptic nature in its mathematical behavior, was involved in the problem. However, its accuracy was strongly dependent on the type of unknown temperature distribution. When some discontinuities were present, the solution accuracy was severely deteriorated, and locations of measurement points were also observed to influence the accuracy. As the measurement positions are located far away, the results became more inaccurate, since the effects of measurement points on unknown wall temperature became poor.

REFERENCES

1. C. H. Huang and M. N. Özisik, Inverse Problem of Determining Unknown Wall Heat in Laminar Flow through a Parallel Plate, *Numer. Heat Transfer A*, vol. 21, pp. 55–70, 1992.

2. H. Y. Li and W. M. Yan, Inverse Convection Problem for Determining Wall Heat Flux in Annular Duct Flow, *ASME J. Heat Transfer*, vol. 122, pp. 460–464, 2000.
3. H. Y. Li and W. M. Yan, Identification of Wall Heat Flux for Turbulent Forced Convection by Inverse Analysis, *Int. J. Heat and Mass Transfer*, vol. 46, pp. 1041–1048, 2003.
4. F. B. Liu and M. N. Özisik, Estimation of Inlet Temperature Profile in Laminar Duct Flow, *Inverse Problems in Eng.*, vol. 3, pp. 131–141, 1996.
5. J. C. Bokar and M. N. Özisik, Inverse Analysis for Estimating the Time Varying Inlet Temperature in Laminar Flow Inside a Parallel Plate Duct, *Int. J. Heat and Mass Transfer*, vol. 38, pp. 39–45, 1995.
6. H. M. Park and O. Y. Chung, An Inverse Natural Convection Problem of Estimating the Strength of a Heat Source, *Int. J. Heat and Mass Transfer*, vol. 42, pp. 4259–4273, 1999.
7. H. Y. Li, Estimation of Thermal Properties in Combined Conduction and Radiation, *Int. J. Heat and Mass Transfer*, vol. 42, pp. 565–572, 1999.
8. H. M. Park and T. Y. Yoon, Solution of the Inverse Radiation Problem Using a Conjugate Gradient Method, *Int. J. Heat and Mass Transfer*, vol. 43, pp. 1767–1776, 2000.
9. H. M. Park and D. H. Yoo, A Multidimensional Inverse Radiation Problem of Estimating the Strength of a Heat Source in Participating Media, *Int. J. Heat and Mass Transfer*, vol. 44, pp. 2949–2956, 2001.
10. K. W. Kim and S. W. Baek, Inverse Surface Radiation Analysis in an Axisymmetric Cylindrical Enclosure using a Hybrid Genetic Algorithm, *Num. Heat Transfer A*, vol. 46, pp. 367–381, 2004.
11. H. Y. Li, An Inverse Source Problem in Radiative Transfer for Spherical Media, *Numer. Heat Transfer B*, vol. 31, pp. 251–260, 1997.
12. Y. K. Hong and S. W. Baek, Inverse Analysis for Estimating the Unsteady Inlet Temperature Distribution for Two-Phase Laminar Flow in a Channel, *Int. J. Heat and Mass Transfer*, vol. 49, pp. 1137–1147, 2006.
13. Y. K. Hong and S. W. Baek, Inverse Radiation Problem in Determination of the Inlet Temperature Profile for Two-Phase Laminar Flow in a Channel, *Numer. Heat Transfer, Part A*, vol. 50, pp. 1–19, 2006.
14. M. Necati Özisik and Helcio R. B. Orlande, *Inverse Heat Transfer*, Taylor and Francis, New York, chap 1–4, 2000.
15. M. F. Modest, *Radiative Heat Transfer*, pp. 295–320 & 541–569, McGraw-Hill, New York, 1993.
16. G. Poot, Heat Transfer by Laminar Free Convection in Enclosed Plane Gas Layers, *The Quarterly J. Mech. and Appl. Math.*, vol. 11, pp. 257–273, 1958.